The Innovation, Volume *3*

Supplemental Information

Achieving ultra-stable and superior electricity generation by integrating transistor-like design with lubricant armor

Yuxin Song, Wanghuai Xu, Yuan Liu, Huanxi Zheng, Miaomiao Cui, Yongsen Zhou, Baoping Zhang, Xiantong Yan, Lili Wang, Pengyu Li, Xiaote Xu, Zhengbao Yang, and Zuankai Wang

Supplemental Data Items

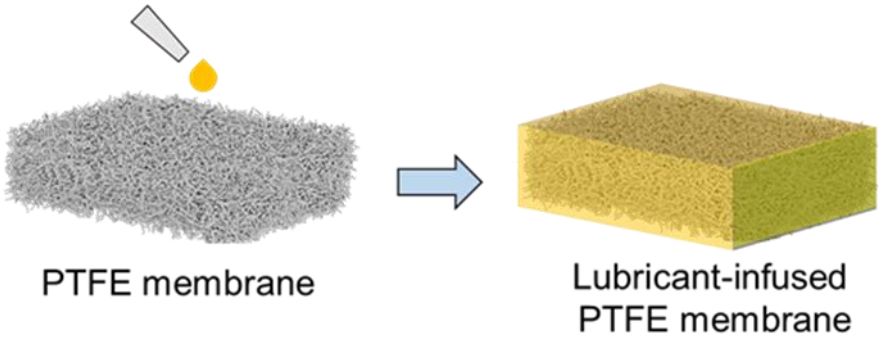

Figure S1. Schematics showing the fabrication of the SLIPS layer.

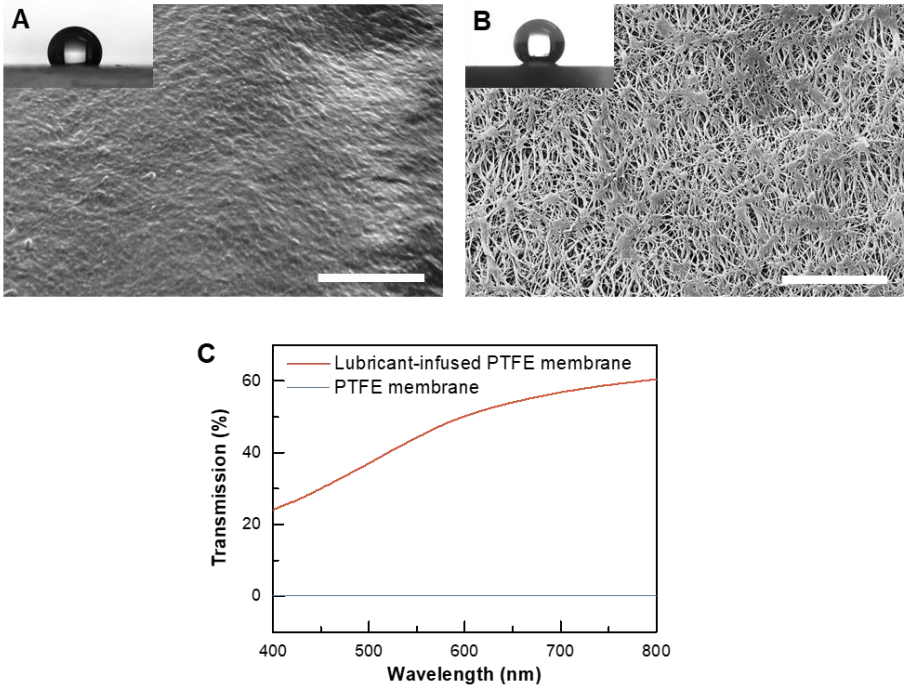

Figure S2. Structure, wettability and optical characterization of SLIPS and PTFE membrane.

(A) SEM image (top view) of SLIPS shows smooth and liquid-like morphology. Inset image measures a static contact angle of 124.4° ± 1.72°. (Scale bar, 30 μm)

(B) SEM image (top view) of PTFE membrane shows nano-porous morphology. Inset image measures a static contact angle of 153.9° ± 3.11° (Scale bar, 10 μm).

(C) Optical transmittance of SLIPS and PTFE membrane.

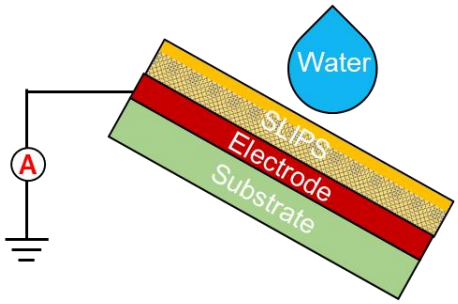

Figure S3. The structure of SLIPS TENG consisting of a SLIPS layer and a single electrode.

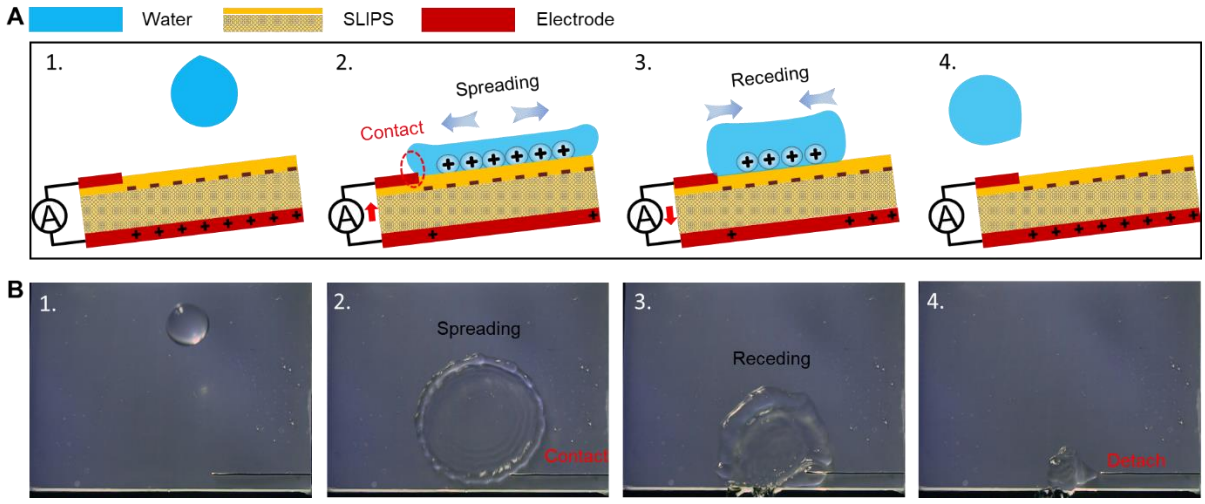

Figure S4. Schematics and snapshots of electricity generation in LA-TEG.

(A) 1. Before a droplet contacts the SLIPS in LA-TEG, all countercharges induced by the surface charges on SLIPS locates at the bottom electrode, resulting in a great potential difference across the SLIPS layer. 2. Once a droplet spreads and bridges the top electrode and SLIPS into a closed-circuit, the electrostatically induced higher potential on bottom electrode as opposed to the SLIPS leads to the building of an electric field, driving the flow of countercharges from the bottom electrode to the top electrode to generate the electricity output. Meanwhile, counter-charged ions in water are driven to screen the surface charge of SLIPS. 3. Then the droplet begins receding and the contact area between water and SLIPS is reduced, resulting in the flow of countercharges back to bottom electrode. 4. When the droplet slides downhill and detaches from top electrode, the circuit becomes open and all charges flow back to the bottom electrode, ready for the electricity generation from next falling droplet.

(B) Snapshots of dynamic droplet impacting process on LA-TEG corresponding to the electricity generation process.

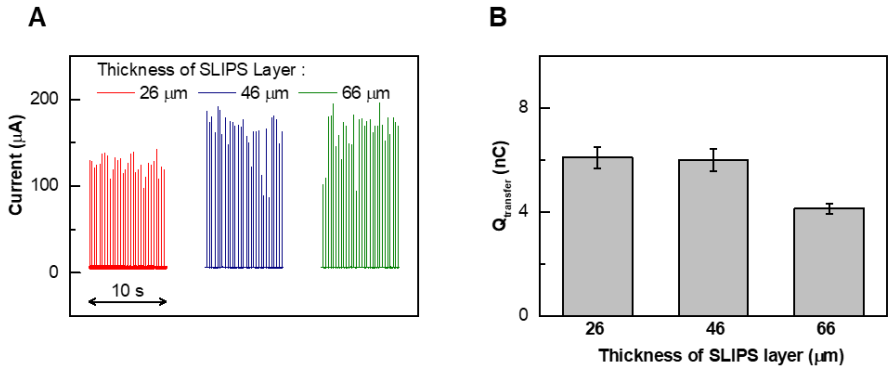

Figure S5. Electrical performance of LA-TEG with the varied thickness of SLIPS layer. (A-B) Output voltage and transfer charge of LA-TEG with the varied thickness of SLIPS layer ranging for 26 μm to 66 μm. (Tap water droplet volume of 50 μL and release height of 12 cm)

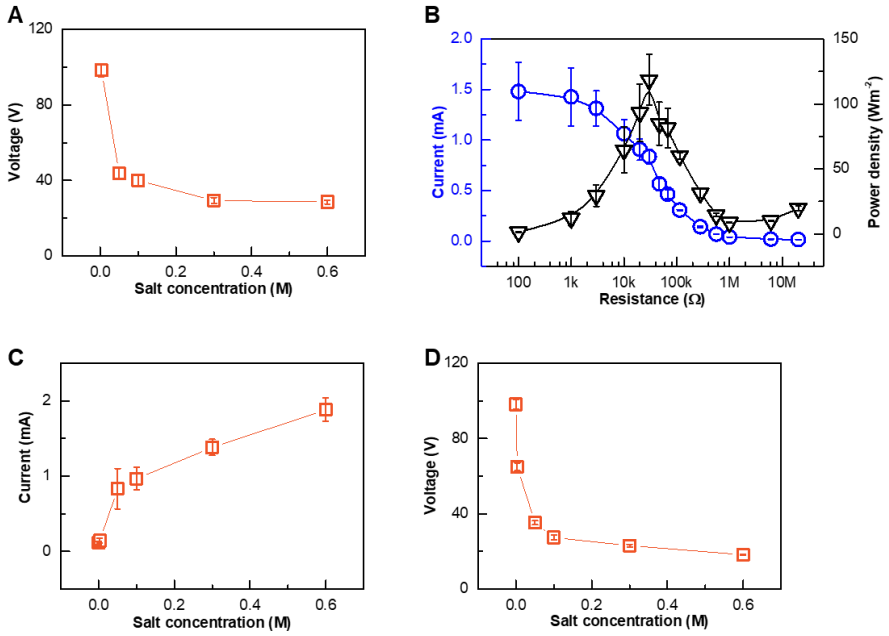

Figure S6. Electrical performance of LA-TEG under continuous impingement of saltwater droplets.

(A) The output voltage of LA-TEG with SLIPS thickness of 46 μm under varied salt concentrations.

(B) Instantaneous power density of the LA-TEG under 0.1M Nacl solution as a function of loading resistance. (SLIPS layer of 46 μm, water droplet volume of 50 μL, release height of 12 cm)

(C) Increased output current of LA-TEG with the increased salt concentrations of water. The thickness of SLIPS layer is 26 μm

(D) The output voltage of LA-TEG with SLIPS thickness of 26 μm under varied salt concentrations.

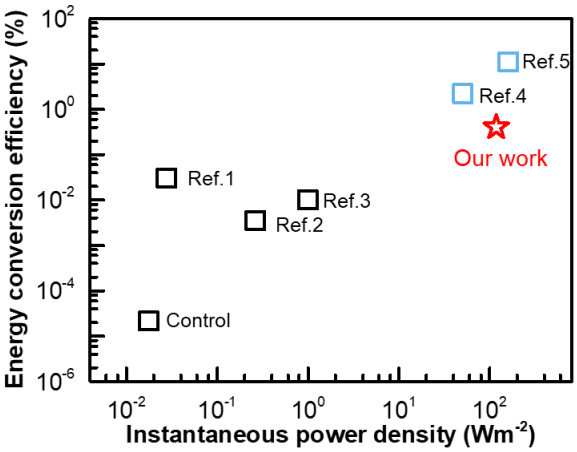

Figure S7. The energy conversion efficiency of our work and some previous work. Our work, TENGs[1-3] and other DEGs[4,5] are represented in red, blue and black, respectively. We demonstrate that our work shows the most stable energy conversion efficiency of 0.4% in spite of the relative low value compared to the generator without the use of SLIPS. Such a stable energy conversion efficiency endowed by the SLIPS facilitates the further practical applications of our design.

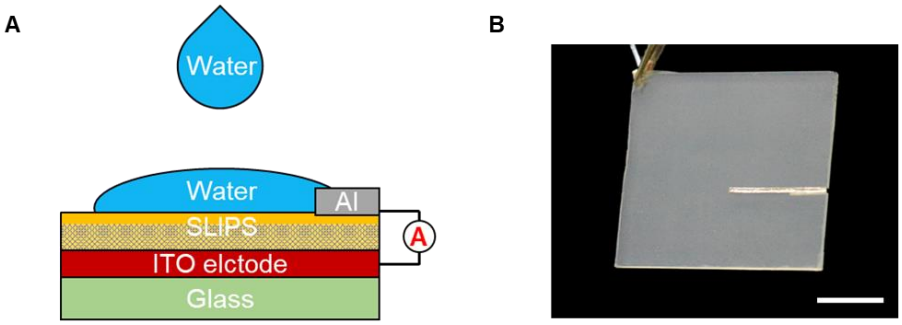

Figure S8. LA-TEG prepared for the stability test.

(A) The LA-TEG consisting of the SLIPS layer, ITO conductive glass and aluminum electrode.

(B) Optical image of the ITO-based LA-TEG.

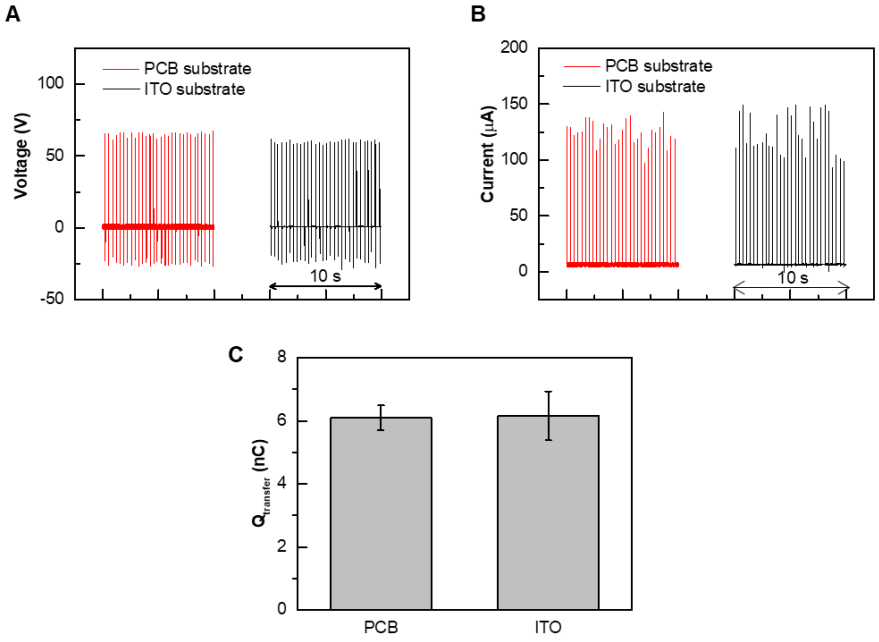

Figure S9. The output voltage, current and transfer charge of the PCB-based and ITO-based LA-TEGs without the extra charging treatment.

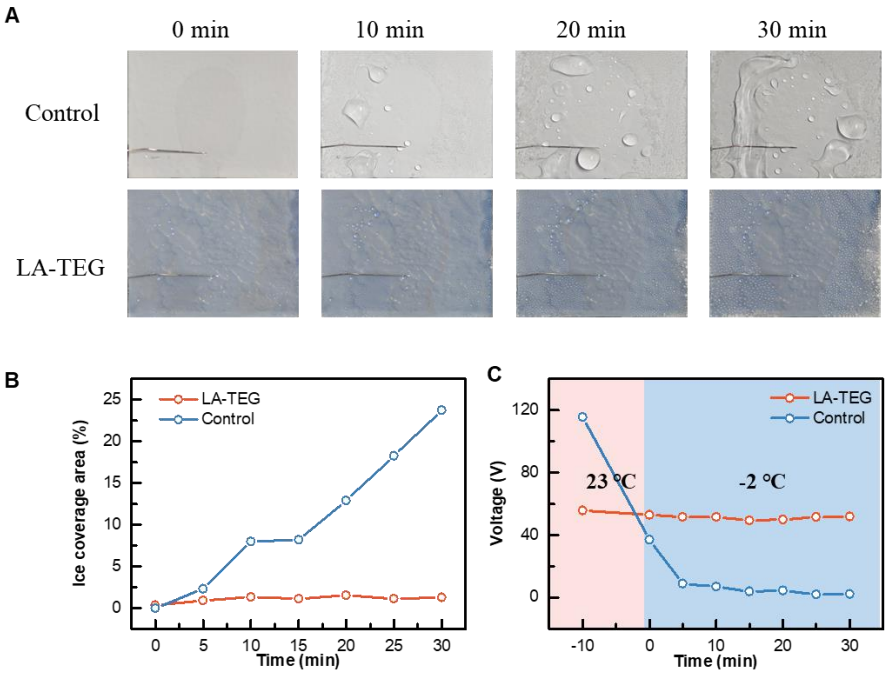

Figure S10. The electrical performance stability of the LA-TEG in the freezing temperature.

(A) Snapshots of icing process on surfaces of LA-TEG and the control sample at -2 ℃. No ice was observed on the LA-TEG while the ice coverage area gradually increased on control surface over time because the lubricant layer can effectively delay ice/frost formation and enhance droplet mobility.

(B) Ice coverage ratio of LA-TEG and control sample at -2 ℃.

(C) Time variation of the LA-TEG's output voltage signal at -2 ℃.

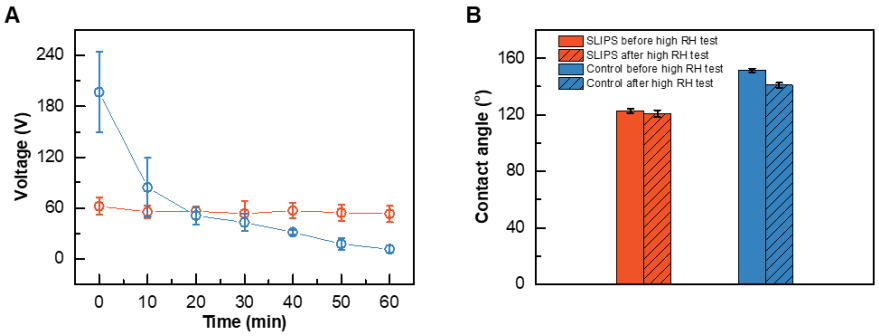

Figure S11. The electrical performance stability of the LA-TEG in the highly humid environment.

(A) Time variation of the LA-TEG's output voltage signal at relative humidity of 100%.

(B) The contact angles of LA-TEG before and after the high humidity test.

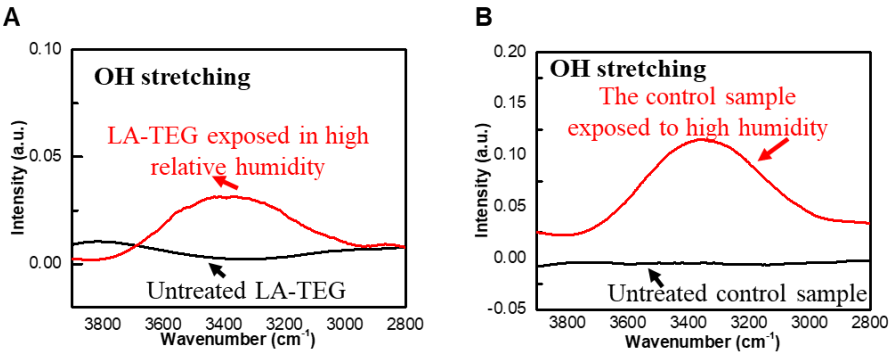

Figure S12. FTIR spectra of the LA-TEG and control sample surfaces prepared under different conditions. Dried samples (black curves) were previously stored under dry conditions. The red curves correspond to test samples that were previously exposed to water vapor. The FTIR spectra of the control sample without the use of lubricant exhibit more strong bands at ca. 3500 cm^{-1}, which is assigned to the stretching vibrational modes of water, suggesting that more water is absorbed on the surface of the control sample than that of LA-TEG.

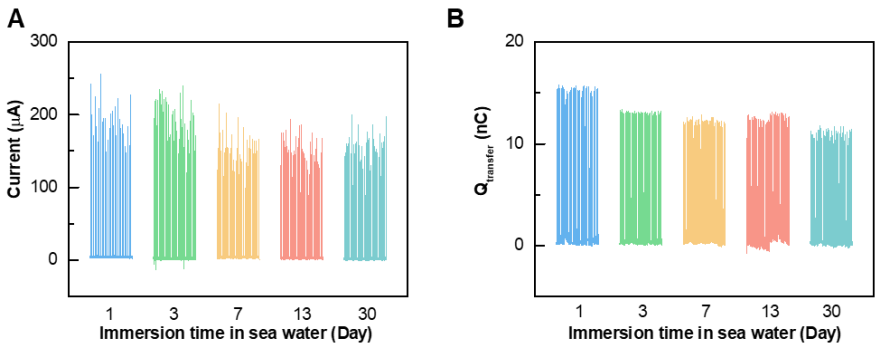

Figure S13. Electrical performance of LA-TEG after the immersion treatment in seawater for 30 days.

(A and B) The time-dependent variation of output current and transfer charge of LA-TEG. The LA-TEG was precharged with a large charge density before the test.

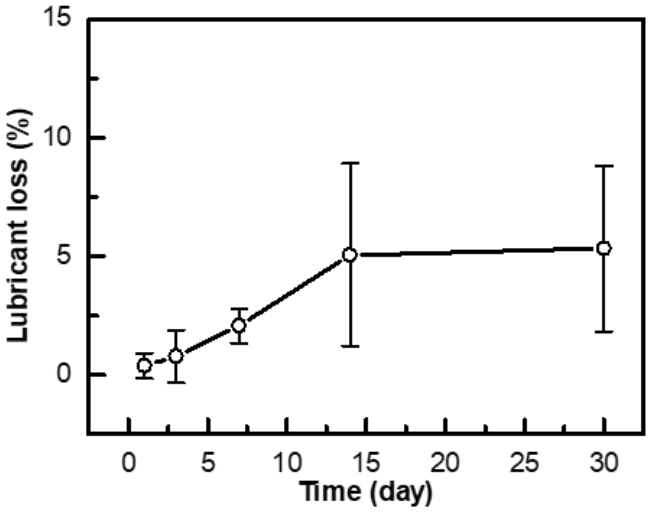

Figure S14. The lubricant loss in LA-TEG when immersed in seawater. There is only 5% loss in the lubricant mass after immersion treatment for 30 days, indicating a long-term durability of the lubricant layer in seawater

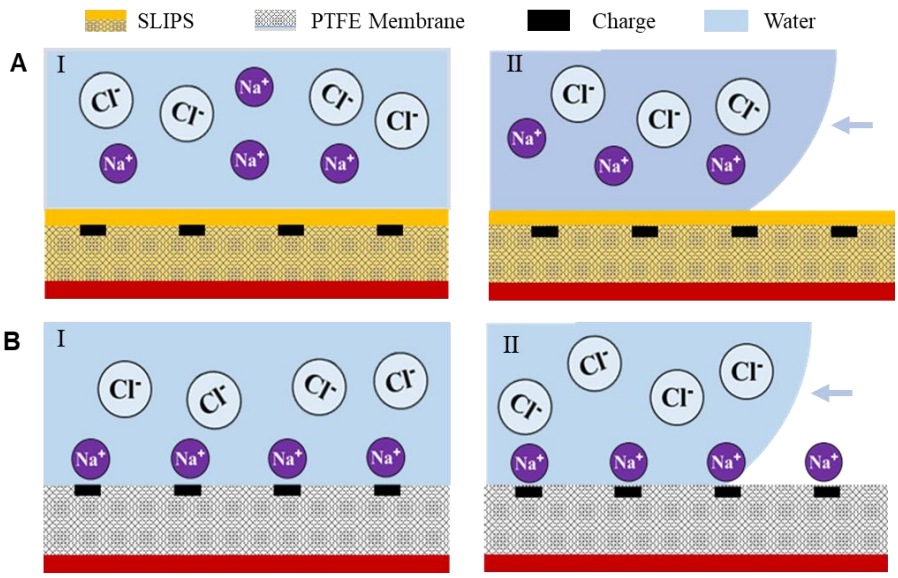

Figure S15. Schematics showing the prevention of ion absorption on LA-TEG using a SLIPS layer.

(A) When LA-TEG is immersed into the solution, the lubricant layer acts as a natural barrier and prevents the lodging of those ions attracted by the negative surface charge on SLIPS. Simultaneously, the lubricant can also mitigate the counter-ion absorption due to its intrinsic fluidity as well as chemical inertia.

(B) Without the use of the lubricant armor, the ions in water can be firmly absorbed onto the PTFE surface of the control sample due to the strong electrostatic attraction between the negative surface charges and the counterions. These adsorbed counterions still remain stationary on the PTFE surface even when the solution is completely detached, which thereby screen the surface charges on PTFE.

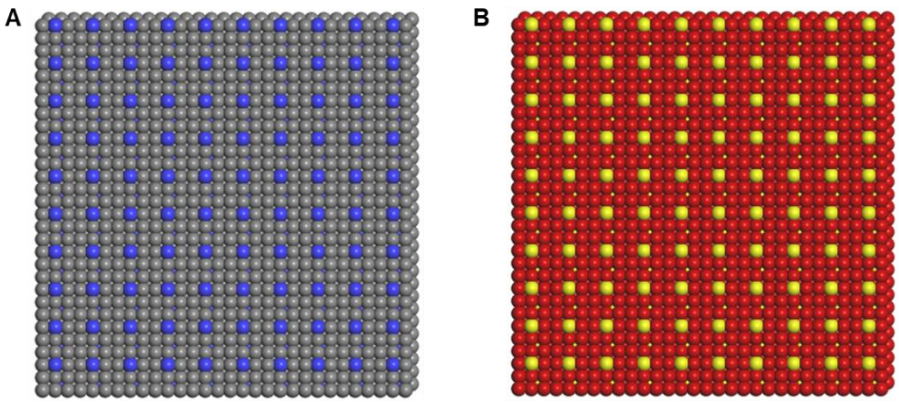

Figure S16. Charge distribution on PTFE and ITO in the models of the systems employed in the Molecular Dynamic (MD) simulations.

(A) 100 negative charges (blue) with decent space are set on the first layer of PTFE (grey).

(B) 100 positive charges (yellow) are fixed on the ITO electrode (red).

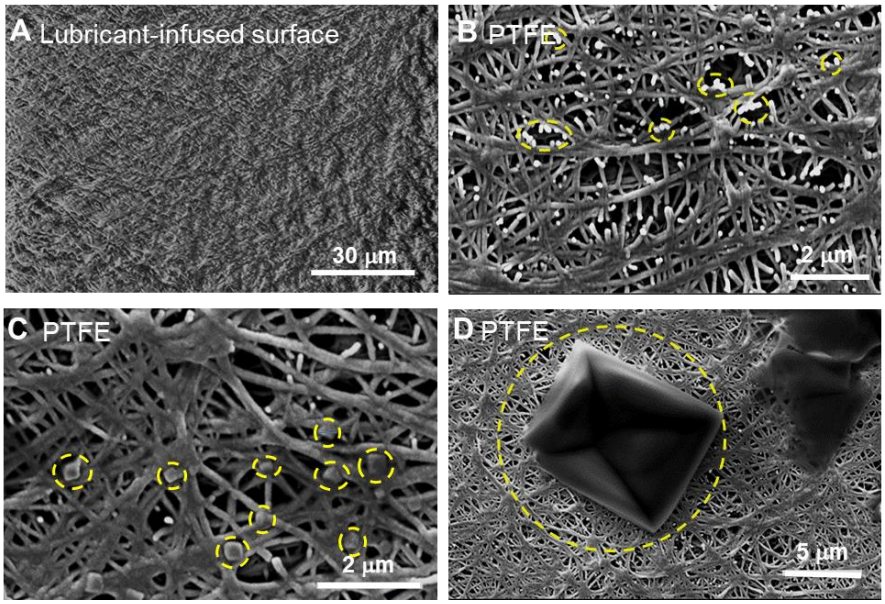

Figure S17. Characterization of salt crystals formed on SLIPS and PTFE surface after immersion in 0.6M NaCl solution for 6 hours.

(A) No salt crystal was observed on the smooth and liquid-like SLIPS.

(B-D) Salt crystals with different sizes ranging from tens nanometers to several micrometers were found on PTFE membrane.

Figure S18. Optical image showing condensed droplets sliding over the condensate energy harvester attached to a curved surface. The condensate energy harvester is made of a SLIPS layer and a flexible printed circuit board integrated with transistor-like electrode architecture.

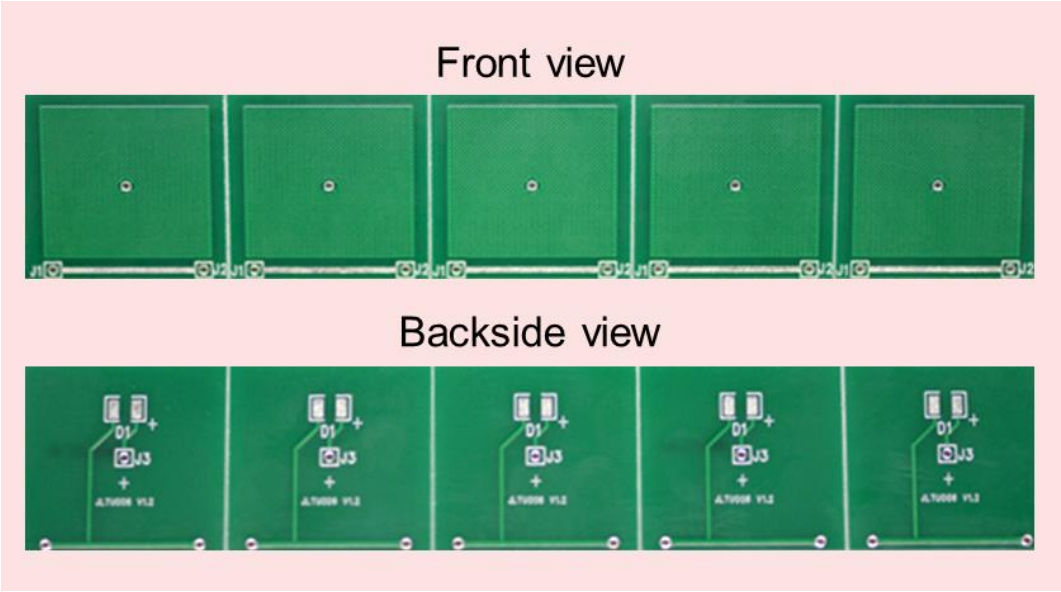

Figure S19. Optical images of the droplet energy harvester consisting of 5 pieces of LA-TEGs.

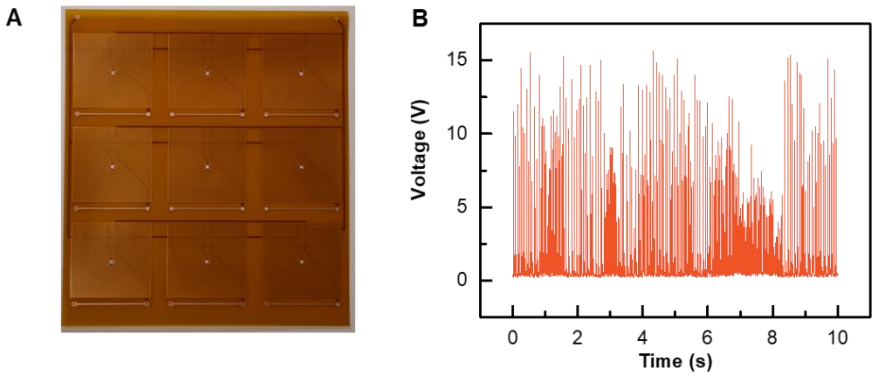

Figure S20. Flow energy harvester.

(A) Optical images of the flow energy harvester consisting of 3×3 pieces of LA-TEGs made by flexible printed circuit boards.

(B) The output voltage of the flow energy harvester under intermittent water flow.

Figure S21. Optical images of the wave energy harvester consisting of 6×5 pieces of LA-TEGs.

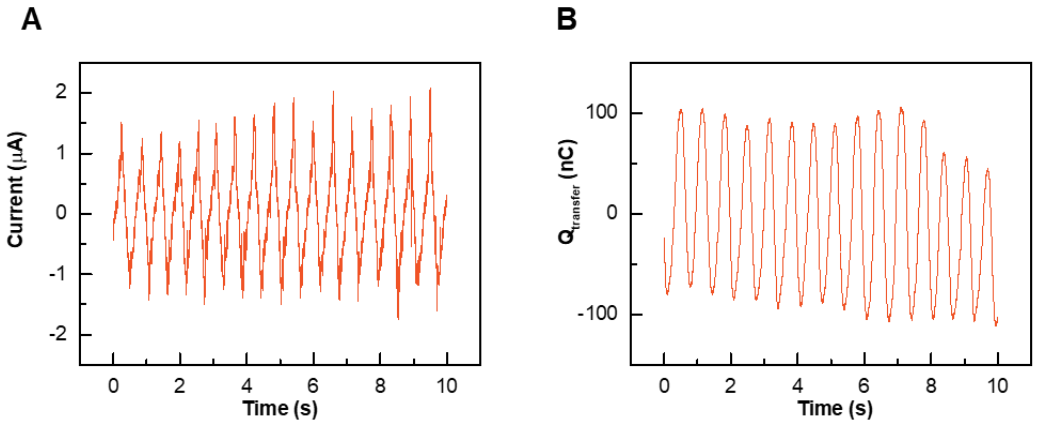

Figure S22. Output current and transfer charge of a wave energy harvester under periodically uprising waves.

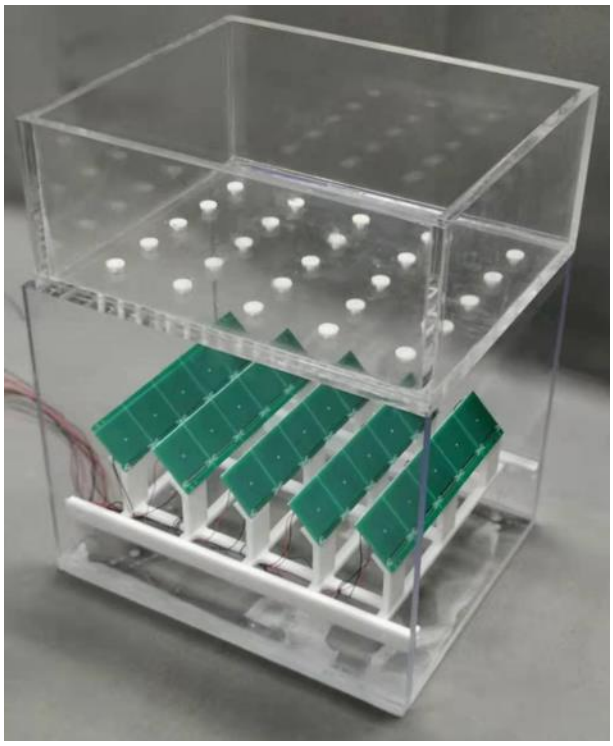

Figure S23. A home-made rain-droplet energy harvest platform is composed of five pieces of droplet energy harvesters, 3D-printed dispensers and sample supports.

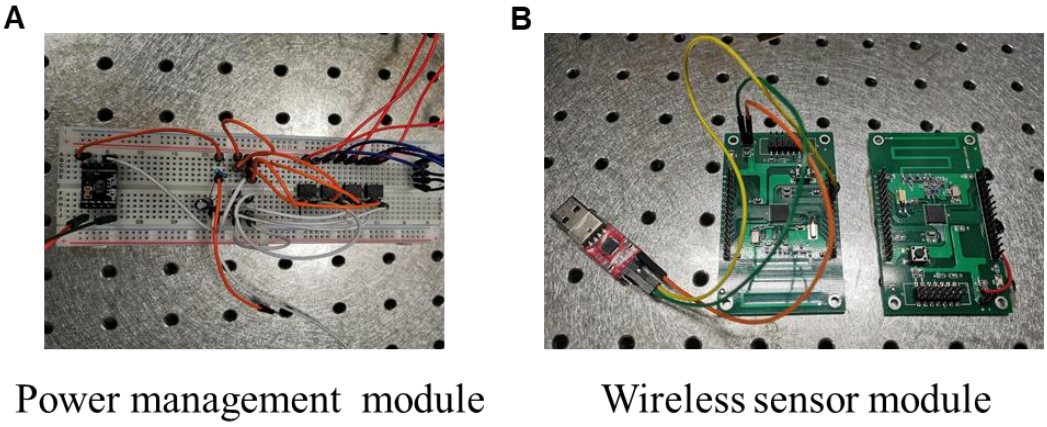

Figure S24. Power management module and wireless temperature sensor module.

(A) The power management module consists of a bridge circuit, a capacitor of 25 μF, and a nanopower energy harvesting power supply (GY-LTC3588).

(B) The wireless temperature sensor module consists of a set of wireless development board (CC430F5137) and a serial to USB adaptor for transmitting signal to the computer.

Note S1

Regulation of lubricant layer thickness and lubricant type

We controlled the thickness of lubricant layer h by the control of volume of lubricant V according to the equation $h = (V-V_{pore})/A=(V-kV_{PTFE})/A$, where A is the area of PTFE membrane and V_{pore} is the volume of lubricant trapped in the pores of the PTFE membrane, which is related to the volume of the PTFE membrane (V_{PTFE}) and the porosity of the membrane (k). As shown in the figure below, the output voltage of LA-TEG gets decreased as the lubricant layer thickness is beyond 7 μm. This is because the thicker lubricant layer will hinder the electrical interaction between the charge carriers in water droplets and surface charge accumulated on the PTFE surface, thus resulting in the inefficient utilization of surface charge for electricity generation. In this regard, we fixed the lubricant layer thickness of LA-TEG as 6 μm in all experiments.

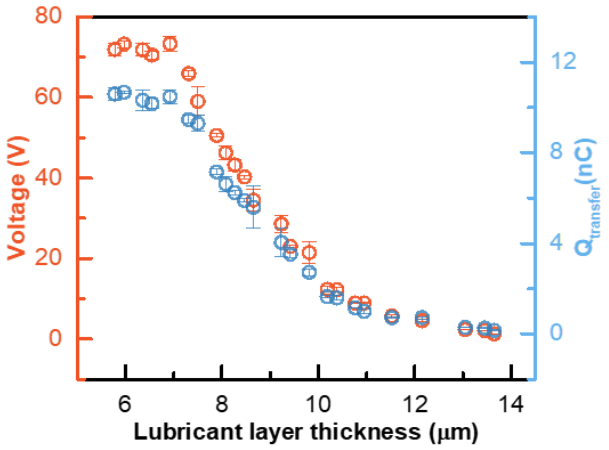

Output voltage and transfer charge as a function of lubricant layer thickness of SLIPS in LA-TEG.

We also investigate the effect of lubricant type on the electrical performance of LA-TEG. As shown in the figure below, Krytox 103 and105 endow LA-TEG with the best performance due to their proper viscosity and relative permittivity. In this regard, Krytox 103 is used in all experiments in this paper owing to its smaller viscosity than Krytox 105.

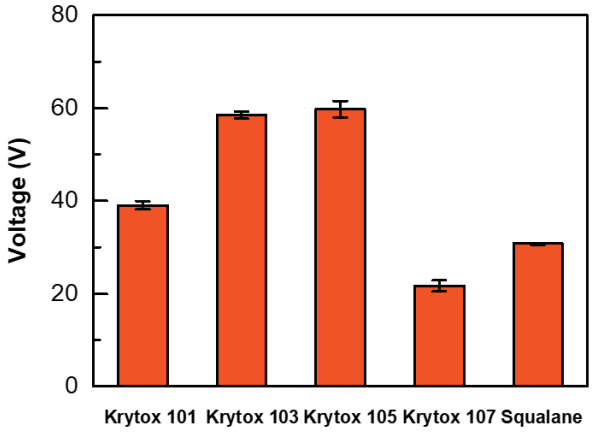

Output voltage of LA-TEG with varied infused lubricants

Note S2

Circuit analysis of LA-TEG.

The dramatic boost of electrical performance of LA-TEG is attributed to the transistor-like design. Since the influence of the charge of droplet itself and dropper can be ruled out, we can shed light on the working mechanism of LA-TEG based on the equivalent circuit analysis. As plotted in the below Figure A, when a water droplet impacts on the surface, LA-TEG can be treated as three serially connected capacitors C_s, C_1 and C_2, respectively. Among them, the capacitor C_s consists of the SLIPS layer (dielectric), SLIPS surface (upper plate), and electrode (bottom plate). The two electric double layer (EDL) capacitors, C_1 and C_2, are formed at the water/SLIPS interface as well as the water/electrode interface, respectively. Water itself can be treated as a resistor in this circuit. In this regard, prior to the contact between water droplet and electrode to form C_2 for charge transportation, the circuit is on an open state without charge transfer. Once the water droplet contacts the electrode, the instant formation of C_2 connect the originally disconnected system to a closed circuit. Therefore, under the giant electric potential induced by the high-density surface charge stored in SLIPS, plenty of charges are forced to transfer in the circuit (Figure B), resulting in an instantaneous peak voltage signal. The equivalent circuit is shown in Figure A, governed by the following differential equation:

$$(R_l + R_w)\frac{dq(t)}{dt} = \frac{Q_S - q(t)}{C_s} - \frac{q(t)}{C_1(t)} - \frac{q(t)}{C_2(t)} \quad (1)$$

$$q(t=0) = 0 \quad (2)$$

where $q(t)$ is the transfer charge, and R_L and R_w are the impedance of the external load and water, respectively. As the thickness of EDL is far smaller than the thickness of SLIPS,$C_s \gg C_1,\ C_2$. Thus, equation (1) can be expressed as:

$$(R_l + R_w)I = \frac{Q_S}{C_s} = V \quad (3)$$

where I is the output current and V is the output voltage of LA-TEG, respectively. In this regard, with a fixed Q_s and C_s, reducing the resistance of water can achieve an improved output current. Introducing the capacitor equation, the output V is governed by the following equation:

$$V = \frac{Q_S}{C_s} = \frac{Q_S d}{\varepsilon S} \quad (4)$$

where d, ε and S represent the thickness, dielectric constant and the surface area of the capacitor C_s. We can conclude that output voltage increases linearly with the SLIPS thickness if Q_s is

constant.

Our analysis can be further validated through the careful synchronization of the droplet spreading dynamic as well as the time-dependent evolution of the output voltage (Figure C and D). When the water droplet contacts the LA-TEG, the system is in a switch-off state and there is no electrical output signal. Then the droplet spreads out and contacts the electrode, transforming the system into a switching-on state. At this critical time t_{on} = 0 s marking the timepoint of water-electrode contact, a pronounced voltage signal emerges with rapid flow of charges from ITO to the electrode. At t_{off} = 0.025 s, the water droplet detaches from the electrode accompanied with the reduction of the voltage signal to zero, indicating that the transferred charges move back to the ITO. Careful inspection of the droplet spreading dynamic on SLIPS shows the contact time of the droplet and electrode is about 25 ms which closely corresponds to the voltage signal duration time $t_{off} - t_{on}$.

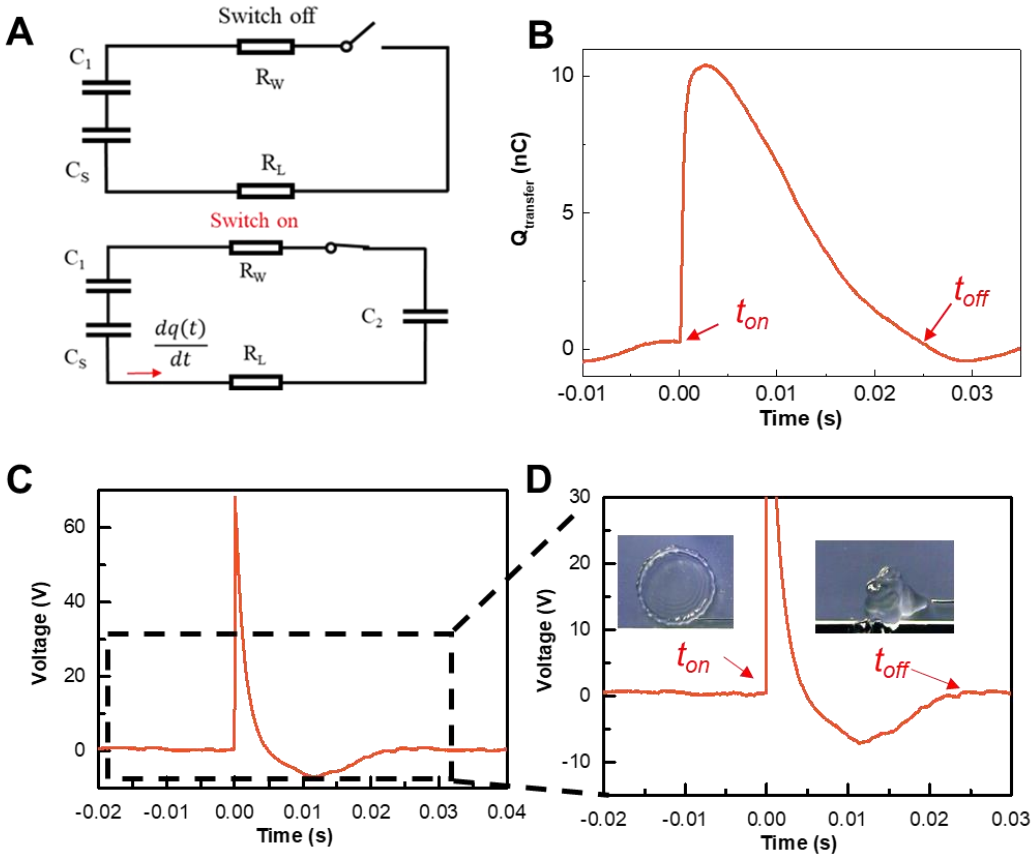

Circuit model and synchronization of droplet-spreading dynamics and voltage response. (A) In the switched-off mode, there is no capacitor formed at the water/top electrode interface because the water droplet has not approached the electrode. As a result, the capacitors C_S and

C_1 remain in an open circuit and there is no charge flow between them. b, Once the water droplet contacts the electrode, the instant formation of capacitor C_2 connect the originally disconnected system to a closed circuit. R_w, R_L and $dq(t)/dt$ in the circuit are, respectively, the impedance of the water droplet, the impedance of the external load and the derivative of the transferred charge with respect to time.

(B) Time-dependent variation in the transferred charge, $Q_{transfer}$, generated on the ITO-based LA-TEG by an impinging droplet, indicating that the process of charge transfer corresponds to the change of the equivalent circuit from switch-on state to switch-off state. The ITO-based LA-TEG was precharged with a large charge density before the test.

(C and D) Synchronization of droplet-spreading dynamics and voltage response of ITO-based LA-TEG. Insets are snapshots showing the snapshots of the droplet dynamics. The ITO-based LA-TEG was precharged with a large charge density before the test.

Note S3

Molecular dynamics simulations.

To investigate the effect of immersion in aqueous solution, we carried out molecular dynamics (MD) simulations. Nanoscale slab models containing about 1.0×104 water molecules with 200 sodium and 200 chlorine ions were employed to simulate the behavior of ions during the immersion processes (Figure S15). To mimic the charged PTFE, rigid atomic layers were used, and negative charges were fixed on the first and second atomic layers with a spacing of 8.7 Å, and equivalent positive charges were fixed on the atomic layers of ITO electrode; each site was charged +e or –e. For the SLIPS case, three more atomic layers were used to represent the lubricant. The box size of the systems was 8.7 nm × 8.7 nm × 30.1 nm, in which the thickness of the aqueous solution was about 4.5 nm. Periodic boundary conditions were applied in the x and y directions. The intermolecular interactions among water molecules were described by using TIP4P/ICE potential. The parameters of Na+ and Cl- are σNa=2.876 Å, εNa=0.5216 kJ/mol, σCl=3.785 Å, εCl=0.5216 kJ/mol as reported in previous work. The cross Lennard-Jones interaction parameters between water and sodium and chlorine ions were obtained based on Lorentz-Berthelot rule. The interactions between substrate atoms (sub) and NaCl water solution were described in the form of 12-6 Lennard-Jones potential with parameters of $\sigma Na\text{-}sub$=3.021 Å, $\varepsilon Na\text{-}sub$=0.4785 kJ/mol, $\sigma Cl\text{-}sub$=3.476 Å, $\varepsilon Cl\text{-}sub$=0.4785 kJ/mol, and $\sigma O\text{-}sub$=3.458 Å, $\varepsilon O\text{-}sub$=0.6223 kJ/mol. Leap-frog algorithm was selected for the integration of newton's equations of motion in the MD simulations with a time step of 1 fs. Fast smooth particle-mesh Ewald method was used for electrostatic interactions with a real-space cutoff 10 Å. The van der Waals interactions were truncated at 10 Å. Nosé-Hoover scheme was employed to control the system temperature at 300 K. All the MD simulations were carried out by using Gromacs 4.5.5 software. First, the aqueous solution with Na^+ and Cl^- were running to reach equilibrium at 300 K without any charges fixed on the substrates. Next, we performed constant-temperature and constant-volume (NVT) MD simulations of the immersion processes for both Control and SLIPS in the time of 50 ns.

Experimental Procedures

Materials.

Hydrochloric acid, Sodium hydroxide, Sodium chloride, Potassium Chloride, Lithium Chloride, Acetone (RCI Labscan, 99,5%), ethanol (Sigma Aldrich, 97%), deionized water, seawater (obtained from Victoria Harbour, Hong Kong), Krytox perfluoropolyether oils (Chemours, GPL 101, 103, 105, 107), and Squalene (J&K Scientific Ltd., 97%) were used without further purification. The dimension of purchased Indium Tin Oxide (ITO) glass (Huananxiangcheng Technology Ltd.) are 3.0 cm×3.0 cm×1.0 mm. The thickness and average pore size of porous PTFE membrane (Sterlitech Corporation, PTU023001) are 20 μm and 200 nm, respectively. PCB substrates with the transistor-like electrode structure were provided by a commercial company.

Fabrication of the LA-TEG.

To fabricate the LA-TEG, a PCB substrate was first ultrasonically cleaned in ethanol for 10 min. Then we gently covered a porous PTFE membrane onto the PCB substrate. To ensure a good contact between the PTFE membrane and PCB substrate, the membrane was first wetted by ethanol with the help of the capillary wicking effect. After the evaporation of the ethanol, several droplets of low-surface-tension Krytox GPL 103 (γ =16–20 mN/m) were dripped onto the membrane to wick into the pores of the PTFE to form a SLIPS layer. All the samples were placed horizontally on a flat table for about 12 hours to allow spontaneous impregnation of lubricant prior to any experimental characterization or measurement.

Fabrication of ITO-based LA-TEG

To fabricate the ITO-based LA-TEG, a piece of ITO glass slide was first ultrasonically cleaned in acetone and ethanol for 10 min, respectively. Then we gently covered a porous PTFE membrane onto the ITO glass followed by rubbing the membrane with the nitrile butadiene rubber for a charging treatment. Then we dropped several droplets of lubricants onto the charged membrane to fabricate the SLIPS layer. After that, a tapered aluminum electrode was attached to the SLIPS layer to construct the transistor-like electrode architecture. For comparison, we fabricated a control sample without the infusion of the lubricant using the

similar method. Also, we fabricated a SLIPS-TENG without the infusion of the lubricant but without attaching the aluminum electrode.

Characterization and Electrical Measurement.

The optical transmittance was measured by using Perkin Elmer Lanbda 35 UV-VIS Spectrometer. Fourier-transform infrared (FT-IR) spectra were recorded using a Bruker Tensor 27 FT-IR Spectrometer with the attenuated total reflectance (ATR) accessory at a resolution of 4 cm^{-1} in the range of 4000-600 cm^{-1}.

We utilized a syringe pump and a plastic tube to form waterjet with the untreated tap water if there is no special instruction. The inner diameter of the plastic nozzle connecting to the outlet of the plastic tube is 1.65 mm, and the corresponding water droplet volume is 50 μL. If not specified, the substrate tilt angle and the release height of water droplet were fixed at 45° and 12 cm, respectively. The impact dynamic wetting behaviors of water droplets were recorded by a high-speed camera (Photron FASTCAM SA4) at a rate of 6,000 frame per second. An oscilloscope (Rohde and Schwarzrte, RTE1024) with a high-impedance (10 MΩ) probe was used for measuring the voltage output of all the devices. We measured the current and transferred charge using a low-noise current preamplifier (Stanford Research System Model SR570) or a nanocoulomb meter (Monroe model 284) coupled with the oscilloscope, respectively. Specially, for testing the behavior of TENGs at low temperature, any sample (LA-TEG or control) was stuck to a thermoelectric cooling stage, that was used to precisely control the sample surface temperature. All the experiments were carried under the ambient relative humidity of 60% and ambient temperature of 25℃ except for the test of samples in low temperature of -2℃ and high humidity of 100%.

Calculation of energy conversion efficiency and power density

As for a PCB-based LA-TEG unit, an electrical energy E of 0.236 μJ can be generated under a falling droplet impact. The kinetic energy of the droplet E_d is 58.8 μJ ($E_d = mgh$, m = 50 mg, h = 12 cm). Thus, the energy efficiency of the device is 0.4%.

The output power density of LA-TEG unit is calculated as $P_s=I^2R/S$, where P_s, I, R and S represent the output power density, output current, the external resistance and the spreading

area of a droplet impacting on LA-TEG, respectively. Noted that the spreading area of a impacting droplet (50 μL and releasing height of 12 cm) is around 1.78 cm^2 measured through the high-speed imaging.

Reference

1 Liang, Q., Yan, X., Liao, X. & Zhang, Y. Integrated multi-unit transparent triboelectric nanogenerator harvesting rain power for driving electronics. *Nano Energy* **25**, 18-25 (2016).

2 Jeon, S.-B., Kim, D., Yoon, G.-W., Yoon, J.-B. & Choi, Y.-K. Self-cleaning hybrid energy harvester to generate power from raindrop and sunlight. *Nano Energy* **12**, 636-645 (2015).

3 Lin, Z. H., Cheng, G., Lee, S., Pradel, K. C. & Wang, Z. L. Harvesting water drop energy by a sequential contact-electrification and electrostatic-induction process. *Advanced Materials* **26**, 4690-4696 (2014).

4 Xu, W. *et al.* A droplet-based electricity generator with high instantaneous power density. *Nature* **578**, 392-396 (2020).

5 Wu, H. *et al.* Charge Trapping-Based Electricity Generator (CTEG): An Ultrarobust and High Efficiency Nanogenerator for Energy Harvesting from Water Droplets. *Adv Mater* **32**, e2001699, doi:10.1002/adma.202001699 (2020).